ACS Catalysis

Research Article

pubs.acs.org/acscatalysis

Electrocatalytic System for the Simultaneous Hydrogen Production and Storage from Methanol

Jesús González-Cobos,[†,§] Víctor J. Rico,[‡] Agustín R. González-Elipe,[‡] José Luis Valverde,[†] and Antonio de Lucas-Consuegra*[,†]

[†]Department of Chemical Engineering, School of Chemical Sciences and Technologies, University of Castilla-La Mancha, Ave. Camilo José Cela 12, 13005 Ciudad Real, Spain

[‡]Laboratory of Nanotechnology on Surfaces, Institute of Materials Science of Seville (CSIC-Uni. Seville), Ave. Américo Vespucio 49, 41092 Seville, Spain

Supporting Information

ABSTRACT: This paper reports a groundbreaking approach for simultaneous hydrogen production and storage that entails catalysis, electrochemistry, surface science, and materials synthesis. A novel electrocatalytic system is developed based on nickel nanocolumnar films of controlled microstructure prepared on K-βAl_2O_3 solid electrolyte supports by oblique angle physical vapor deposition. The outstanding characteristics of this system are a hydrogen storage capacity of up to 19 g of H_2 (100 g of Ni)$^{-1}$, which is unparalleled in the literature and the possibility of controlling its release electrochemically, under fixed mild conditions (280 °C and normal pressure). H_2 is produced in situ by methanol steam re-forming on the Ni catalyst, and it spills over onto graphene oxide aggregates formed during the catalytic process, as confirmed by SEM, FTIR, and Raman spectroscopy. The proposed storage mechanism considers a synergetic contribution of both Ni and graphene oxide, promoted by K^+ ions, in enhancing the hydrogen storage capacity of the system.

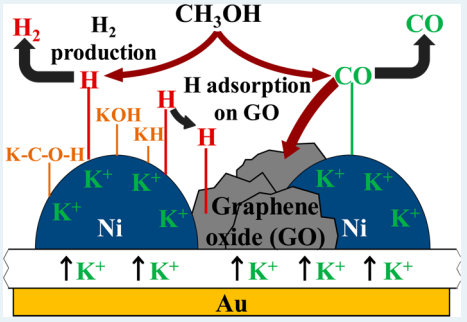

KEYWORDS: *hydrogen storage, methanol re-forming, graphene oxide, alkali promotion, nickel nanorods, glancing angle deposition*

1. INTRODUCTION

Hydrogen is a very important feedstock in the chemical industry and a promising energy carrier with main applications in internal combustion engines and fuel cell technology, where it can be an alternative to the massive consumption of fossil fuels. H_2 presents a very high gravimetric energy density and can be considered an environmentally friendly fuel, provided that both the energy and the raw material employed for its production are sustainable.[1] To date, hydrogen is mainly obtained via methane steam re-forming or water electrolysis, although the catalytic conversion of hydrogen liquid carriers such as alcohols is acquiring an increasing interest.[2,3]

Owing to the low volumetric energy density of gaseous H_2, the development of efficient hydrogen storage systems is of paramount importance for its effective handling. In addition to the conventional H_2 storage in the form of compressed gas or cryogenic liquid, most storage procedures can be grouped into two main categories: physisorption of molecular H_2 and chemisorption of atomic hydrogen.[4−6] In the first case, adsorbents such as carbon materials, metal−organic frameworks (MOFs), covalent organic frameworks (COFs), porous polymers, and zeolites have shown fast H_2 adsorption kinetics and good reversibility, although their practical use is hampered by their typically low H_2 storage capacity (around 5 wt % at −196 °C). In the second case, atomic hydrogen chemisorption may lead to the formation of chemical compounds, such as metal hydrides, although those providing high storage capacities, e.g., $LiBH_4$ (18 wt % H_2), usually require high decomposition temperatures (up to 600 °C) and present problems of storage reversibility.

The H_2 storage capacity of systems based on metal catalysts such as Pt, Pd, or Ni is commonly increased by using some metal oxide or carbonaceous support[7−9] where H atoms may spill over after hydrogen chemisorption on the active metal phase from either a gaseous stream (as H_2) or a liquid electrolyte (electrochemically, i.e., as H^+). Carbonaceous structures containing oxygen-rich functional groups, such as graphite oxide[9,10] and graphene oxide,[11,12] are especially suited for this purpose. Hydrogen diffused from the metal catalyst (source of H spillover) has been effective in yielding reduced graphene oxide (RGO) from graphene oxide (GO).[11,12] The interest in this kind of material would be further amplified if, in addition to the high prospects of GO as a precursor for graphene manufacturing and its use in many application fields (e.g., gas sensing,[13] water purification,[14] photocatalysis,[15] oand biotechnology[16]), it could also act as an effective hydrogen storage material.

Received: December 14, 2015
Revised: February 10, 2016
Published: February 19, 2016

DOI: 10.1021/acscatal.5b02844
ACS Catal. 2016, 6, 1942−1951

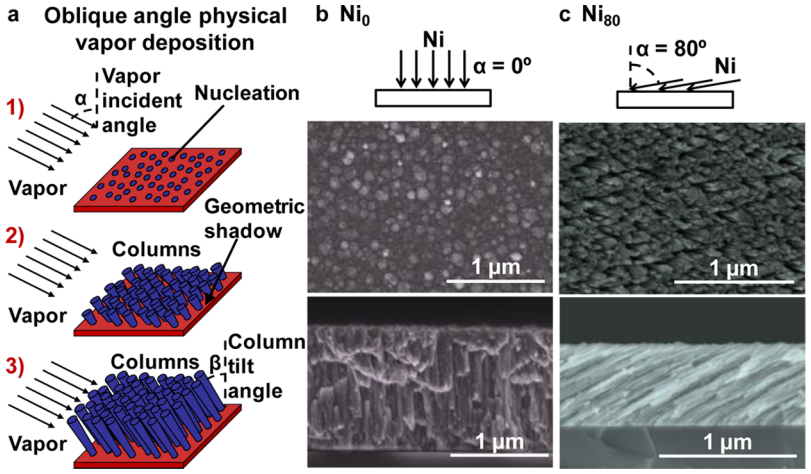

Figure 1. (a) Schematic of the oblique angle physical vapor deposition technique. (b, c) Cross-sectional and top SEM images of the (b) normal and (c) oblique angle deposited Ni catalyst films (Ni_0 and Ni_{80}, respectively) on silicon substrate.

Herein, we develop a novel materials system that first acts as an electrocatalyst for the electrochemically assisted production of H_2 from direct alcohol−water streams at relatively low temperature (i.e., 280 °C) and normal pressure and also operates as an efficient hydrogen storage device. Outstanding properties of this system are a high capacity to store H_2 and the possibility of inducing its release by just switching the catalyst potential, while temperature and pressure conditions are kept fixed. The key issue in sustaining this storage capacity is the architecture of the electrode consisting of a new type of nanostructured catalyst with a high porosity and excellent performance for H_2 production and storage from a humidified methanol stream, as will be observed below. The nanostructured active film consists of tilted Ni nanorods deposited on a K-βAl_2O_3 solid electrolyte by physical vapor oblique angle deposition (PV-OAD), also called glancing angle deposition (GLAD).[17−19] By this method, porosity, morphology, and gas-exposed metal surface area can be enhanced simply by varying the zenithal deposition angle between the evaporation target and the substrate normal.[20−22] In the course of this investigation, it has been found that the unprecedented H_2 storage capacity achieved is linked to the formation of oxygenated graphene during the re-forming reaction. To unravel the H_2 storage and release mechanisms, different ex situ characterization techniques (SEM, XPS, Raman spectroscopy, and FTIR) have been employed. On the basis of the obtained results, we propose that the voltage-driven removal of K^+ ions from the catalyst surface may act as a switching mechanism on the nanostructured nickel film and carbonaceous deposits (i.e., graphene oxide) to induce first the storage and then the controlled release of hydrogen.

2. EXPERIMENTAL METHODS

2.1. Preparation and Characterization of the Electrochemical Catalysts. The electrochemical catalyst consisted of a Ni thin film (geometric area of 2.01 cm^2), which also behaved as the working electrode (W). A 19 mm diameter, 1 mm thick K-βAl_2O_3 (Ionotec) pellet was used as both catalyst support and K^+-conductor material (i.e., as a source of alkali promoter ions). In first place, Au counter (C) and reference (R) electrodes were deposited on one of the sides of the solid electrolyte by applying thin coatings of an organometallic Au paste (Fuel Cell Materials 233001), followed by calcinations at 800 °C for 2 h (heating ramp of 5 °C min^{-1}). The inertness of these two Au electrodes to the methanol steam re-forming reaction was checked via blank experiments. The active Ni catalyst film was then prepared on the opposite side by two different techniques: the classical physical vapor deposition (PVD) method, i.e., in a configuration where vapor particles impinge perpendicularly on the surface of the substrate, and a modification of this technique called oblique or glancing angle deposition (OAD or GLAD). By this method, the substrate (K-βAl_2O_3) is placed in an oblique or glancing angle configuration with respect to the evaporated flux of target material (Ni) to enhance the shadowing effects during the film growth,[17,18,23,24] as schematized in Figure 1. As a result, highly porous films formed by tilted nanocolumns can be obtained, which are characterized by a high gas-exposed surface area and a controlled microstructure depending on the vapor incident angle, the rotation speed of the substrate, and the temperature during the deposition, among other factors. Herein, two types of Ni catalyst films were prepared by applying two different zenithal incident angles. In both cases, Ni target pellets (Goodfellow, 99.9999% purity) were evaporated under vacuum conditions by bombardment with a high kinetic energy (<5 keV) and intensity (150 mA) electron beam. Then, the vapor was condensed onto the surface of the substrate (K-βAl_2O_3) at room temperature. The first catalyst (henceforth denoted as Ni_0) was grown at $\alpha = 0°$ and consisted of a fairly compact Ni film. The second Ni catalyst (denoted as Ni_{80}) was deposited at a zenithal evaporation angle of $\alpha = 80°$ and led to a catalyst film composed of tilted Ni nanocolumns with high porosity (see Figure 1). Both deposited Ni catalyst working electrodes (Ni_0 and Ni_{80}) were electrically conductive. Similar thin films were prepared on silicon substrates for analysis purposes. In the case of this standard substrate (i.e., flat silicon wafers), the nanocolumns grow homogeneously on the entire surface, as shown in the schematic of Figure 1a and in the SEM images of Figure 1b,c. However, the K-βAl_2O_3 surface is rather rough (see Figure S1 in the Supporting Information), with grain sizes of 1−5 μm, i.e., of the same order of magnitude as the Ni film thickness. As a consequence, shadowing effects are higher on this surface, where they lead to a nonuniform column distribution. This point will be further discussed later. The film thickness was estimated from scanning electron microscopy (SEM) analysis using a Hitachi S4800 field emission

DOI: 10.1021/acscatal.5b02844
ACS Catal. 2016, 6, 1942−1951

microscope operated at 2 keV. The final metal loading in the sample grown in a normal configuration was calculated from the SEM analysis and the geometric dimensions of the film. Then, on the basis of this reference loading value, the metal loading in the sample deposited at an oblique angle was determined by X-ray fluorescence (XRF) in a Panalytical spectrophotometer (Model AXIOS) with a rhodium tube as radiation source, by comparison of the total counts obtained for the two samples normalized with the thickness. The measurements were carried out on the samples deposited on the silicon reference substrates and on the K-βAl_2O_3 substrates with a similar result. The obtained Ni/K-βAl_2O_3/Au electrochemical catalysts were placed into a single chamber solid electrolyte cell reactor (Figure 2a) and the three electrodes (working, counter and reference) were connected to an Autolab PGSTAT320-N potentiostat–galvanostat (Metrohm Autolab). Prior to the H_2 production/storage experiments, the catalyst films were subjected to a 2% H_2 stream (Ar balance) while being heated at the working temperature, i.e., 280 °C (ramp of 5 °C min^{-1}), to ensure their reduced state.

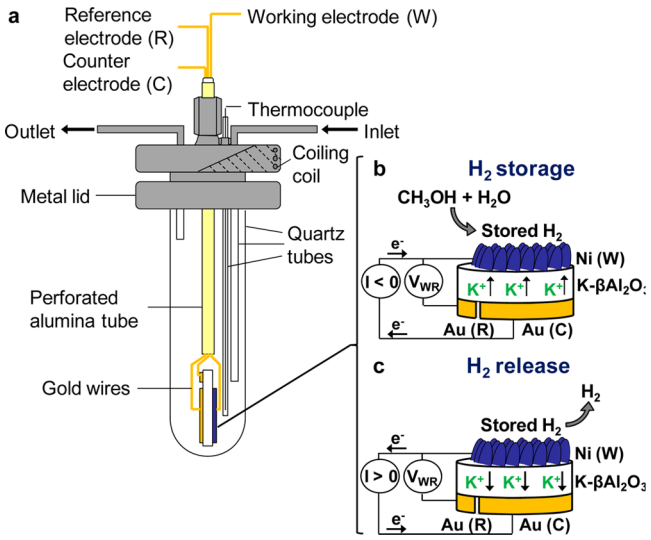

Figure 2. Schematic representations of (a) the single-chamber solid electrolyte cell reactor and the electrochemical catalyst upon (b) cathodic polarization (H_2 storage step) and (c) anodic polarization (H_2 release step).

2.2. Hydrogen Production and Storage Experiments. Each experiment proceeded in four consecutive steps, as follows.

(1) The Ni catalyst film was subjected for 30 min to methanol steam re-forming (SRM) conditions (CH_3OH/H_2O = 4.4%/5.2%, Ar balance, 6 Ndm^3 h^{-1}) at a positive potential, V_{WR} = +2 V, in order to remove all the promoter ions (K^+) that might be located on the catalyst working electrode. The aim of this treatment is to obtain a cleaned Ni catalyst surface as a reference state.

(2) Under the same reaction conditions, a constant negative current, I, was applied for 45 min. In this way, K^+ promoter ions were electrochemically transferred at a constant rate, $r_{K^+} = I/F$ (F being the Faraday constant, 96485 C), from the K-βAl_2O_3 solid electrolyte to the Ni catalyst electrode (Figure 2b), where they may migrate through the entire gas-exposed Ni catalyst surface and/or react with coadsorbed species. The reader is referred to the comprehensive reviews by Vayenas et al.[25] and Vernoux et al.[26]

(3) After the reaction, the reactor was purged with Ar and the system was kept under negative polarization.

(4) Finally, a linear sweep voltammetry (LSV) was performed from −0.6 to +2 V at a scan rate of 1 mV s^{-1} (still under an Ar atmosphere) to decompose the possibly formed potassium-derived surface compounds and to bring the K^+ ions back to the solid electrolyte (Figure 2c). The experiment ended when the release of gas compounds from the catalyst electrode surface vanished.

Methanol (Panreac, 99.8% purity) and water (distilled and deionized) were fed by sparging Ar through thermostated saturators. The reaction gases (Praxair, Inc.) were certified standards (99.999% purity) of Ar (carrier gas) and H_2 (fed in additional experiments). The gas flow rates were controlled by a set of mass flowmeters (Bronkhorst EL-FLOW). All lines placed downstream from the saturators were heated above 100 °C to prevent condensation. Reactant and product gases were analyzed online by using a double-channel gas chromatograph (Bruker 450-GC) equipped with Hayesep and Q-Molsieve 13X consecutive columns and a CP-Wax 52 CB column, along with thermal conductivity (TCD) and flame ionization (FID) detectors, respectively.

2.3. Characterization Measurements after Catalytic Experiments. In order to investigate the composition of the catalyst surface during the H_2 storage process and identify the possible surface compounds formed, the catalyst film Ni_{80} was characterized after the catalytic activity measurements. Prior to the measurements, it was exposed to methanol steam re-forming conditions (CH_3OH/H_2O = 4.4%/5.2%, Ar balance, 6 Ndm^3 h^{-1}) at 280 °C while a negative potential of V_{WR} = −1 V was applied. In this way, K^+ ions electrochemically transferred from the K-βAl_2O_3 solid electrolyte to the catalyst film could favor the H_2 production/storage process, as will be discussed later. After 1 h, the electrochemical catalyst was cooled to 100 °C and the applied potential was interrupted (open-circuit conditions). Then, the catalyst was transferred to the different characterization equipment under inert conditions (i.e., under an N_2 atmosphere). The same procedure was repeated by applying a positive potential of V_{WR} = +2 V under a reaction atmosphere before cooling the reactor.

In addition to SEM, X-ray photoelectron spectroscopy (XPS) was performed with a PHOIBOS-100 spectrometer with Delay Line Detector (DLD) from SPECS, which worked in the constant pass energy mode fixed at 30 eV. Monochromatic Mg Kα radiation was used as the excitation source, and the binding energy (BE) scale of the spectra was referenced to the C 1s signal of graphitic carbon taken at 284.6 eV. The study of the surface compounds was performed through specular reflectance FTIR spectroscopy using a Jasco FT/IR-6200 spectrometer. All spectra were typically obtained using 500 scans with a resolution of 4 cm^{-1}. To remove the background, the signal obtained from a gold substrate was subtracted. Raman spectra were also recorded with a HORIBA HR-800-UV microscope. For these measurements, a green laser (532.14 nm) working at 600 lines per mm and a 100× objective were used.

3. RESULTS

3.1. Catalyst Thin Film Microstructure. For the different experiments carried out in this work, nanostructured porous Ni catalyst films used as working electrodes (Ni_{80}) were prepared at a zenithal angle, α, formed between the perpendicular to the

DOI: 10.1021/acscatal.5b02844
ACS Catal. 2016, 6, 1942−1951

substrate and the evaporation direction, set to 80°. Reference dense Ni films (Ni_0) were also deposited in a normal configuration: i.e., with $\alpha = 0°$. On a flat substrate, the PVOAD technique leads to the formation of highly porous films formed by tilted nanocolumns resulting from shadowing effects produced during the vapor condensation on the surface.[17,18] Figure 1b,c show top view and cross-section SEM micrographs of both Ni_0 and Ni_{80} films, respectively, deposited on flat silicon wafers. The Ni_0 sample consists of a fairly dense film (1.3 μm thick) formed by vertical, thin, and close-packed nanocolumns. One can observe that these Ni_0 nanocolumns present diameters of around 100 nm and a very low porosity and roughness. Unlike this compact morphology, catalyst Ni_{80} consists of a 0.6 μm thick film composed of tilted Ni nanocolumns (tilt angle, $\beta \approx 65°$) with diameters of around 30 nm. They are grouped in the form of bundles of three to five nanocolumns, leaving large void spaces (50−100 nm) between them. A pore fraction of ca. 35% of total volume can be deduced for this sample by considering its thickness and the metal loadings determined by X-ray fluorescence (XRF), i.e., 1.09 and 0.36 mg Ni cm^{-2} for samples Ni_0 and Ni_{80}, respectively. The microstructure of the films, particularly for sample Ni_{80}, opened significantly when they were deposited on the ionic conductor pellet (K-βAl_2O_3) and the homogeneous microstructure found on the silicon substrates transformed into separated nickel nanocolumnar agglomerates (cf. Figure 3a,b). Hence, shadowing effects are higher in Ni films deposited on this substrate, where some regions incorporating a high concentration of metal nanocolumns are surrounded by others with a very low coverage of vaporized material. This phenomenon is depicted in Figure S2a in the Supporting Information. We anticipate that the heterogeneous surface resulting from this enhancement of the shadowing effects due the intrinsic roughness of the K-βAl_2O_3 pellet[27] is a critical factor for the promotion of the hydrogen storage capacity of this electrocatalytic system. Figure 3a,b also shows the strong influence of the vapor incident angle during the film deposition procedure on the final catalyst porosity. The morphology of the oblique angle physical vapor deposited film can be appreciated in more detail in Figure S2b in the Supporting Information. Figure 3c displays a micrograph of Ni_{80} catalyst film after the catalytic experiments and shows that, as discussed in more detail later, carbonaceous deposits are formed during the re-forming reaction. Moreover, the Ni nanocolumns showed the same shape and distribution in Figure 3b,c, thus confirming the good stability of this kind of catalyst film under working conditions, a feature in agreement with previous studies.[28]

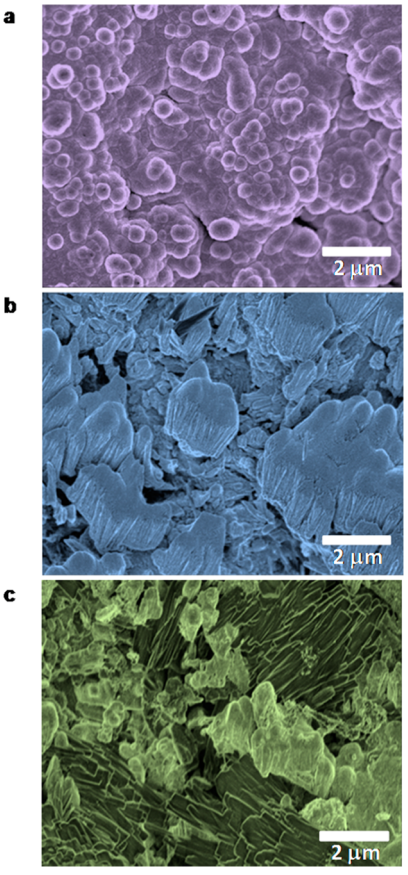

Figure 3. Top view SEM images of catalysts (a) Ni_0 and (b) Ni_{80} as deposited and (c) Ni_{80} after the H_2 production/storage experiments (280 °C, CH_3OH/H_2O = 4.4%/5.2%) and a final application of V_{WR} = −1 V for 1 h.

3.2. Electrochemically Assisted H_2 Storage Experiments. In each experiment, H_2 storage was achieved under methanol steam re-forming conditions (CH_3OH/H_2O = 4.4%/5.2%, Ar balance, 6 $Ndm^3\ h^{-1}$) and application of a constant negative current (I), i.e., upon transferring K^+ ions from the solid electrolyte to the Ni catalyst film. Then, after the reactor was purged with Ar, the release step was induced upon positive polarization: i.e., upon transferring the K^+ ions back to the solid electrolyte. Figure 4 shows the variation with time, during one experiment with catalyst Ni_{80}, of the outlet molar flow rates of the different products, the catalyst potential (V_{WR}) and the current density (j). At $t = 0$, unpromoted H_2, CO, and CO_2 production rates of 6.35×10^{-5} mol of $H_2\ s^{-1}$ (g of Ni)$^{-1}$, 8.5×10^{-6} mol of CO s^{-1} (g of Ni)$^{-1}$, and 2.0×10^{-6} mol of $CO_2\ s^{-1}$ (g of Ni)$^{-1}$ were obtained (Figure 4a). These molar flow values point to that, under the studied reaction conditions, methanol decomposition (MD, eq 1) prevailed over steam re-forming (SRM, eq 2), as commonly found with Ni-based catalysts.[29]

$$CH_3OH \rightarrow 2H_2 + CO \quad (1)$$

$$CH_3OH + H_2O \rightarrow 3H_2 + CO_2 \quad (2)$$

During the application of a constant negative current of $I = -20$ μA (i.e., a current density of $j = -10$ $\mu A\ cm^{-2}$ and a supply of alkali ions to the catalyst electrode at a rate of $I/F = 2.1 \times 10^{-10}$ mol of $K^+\ s^{-1}$, according to Faraday's law), the obtained amount of hydrogen continuously exceeded the theoretical amount which could be expected on the basis of the experimentally observed amounts of CO and CO_2 (from eqs 1 and 2). This feature strongly suggested the accumulation of carbonaceous deposits on the electrode surface. In the course of the catalytic process, both H_2 and CO production rates decreased with time to 3.78×10^{-5} mol of $H_2\ s^{-1}$ (g of Ni)$^{-1}$ and 4.8×10^{-6} mol of CO s^{-1} (g of Ni)$^{-1}$, denoting a certain deactivation of the Ni catalyst which we tentatively attribute to the deposited carbon. After 45 min, when the catalyst potential decreased to ca. −1.2 V and a total amount of 5.6×10^{-7} mol of K^+ was electrochemically transferred to the surface, the steam re-forming reaction was interrupted and all the gas lines and the reactor were fully purged with Ar. Under these conditions, a linear increase of the catalyst potential (V_{WR}) up to +2 V (i.e., inducing the migration of the K^+ ions back to the solid electrolyte; Figure 4b) led to a considerable desorption of H_2

DOI: 10.1021/acscatal.5b02844
ACS Catal. 2016, 6, 1942−1951

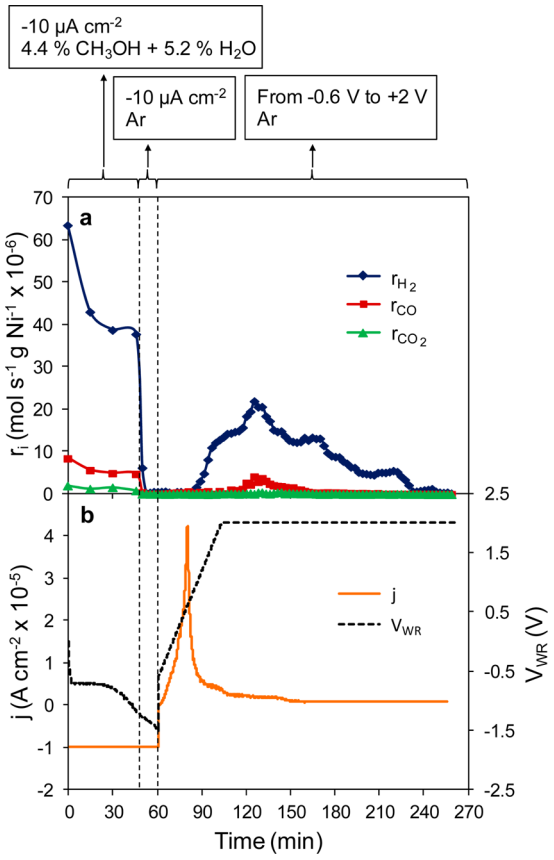

Figure 4. Variation of (a) H_2, CO, and CO_2 molar flow rates and (b) current density (j) and catalyst potential (V_{WR}) with catalyst Ni_{80} during the following steps at 1 atm and 280 °C: CH_3OH/H_2O = 4.4%/5.2%, j = −10 μA cm^{-2} (H_2 production/storage); 100% Ar, j = −10 μA cm^{-2} (cleaning); 100% Ar, linear sweep voltammetry (LSV) from −0.6 V to +2 V at 1 mV s^{-1} (H_2 release).

along with low amounts of CO and CO_2, stemming from previously accumulated surface species. The integration of the peak areas yields a release of 6.80×10^{-5} mol of H_2, 5.6×10^{-6} mol of CO and 8×10^{-7} mol of CO_2 during this anodic scan. These values show that the amount of released H_2 was not only larger than that of the other gas products but also 1 order of magnitude higher than the amount of K^+ ions transferred during the negative polarization step. It is worth noting that the evolution of gases in this step was only detected after the majority of K^+ ions had been brought back to the solid electrolyte (i.e., when the current was approaching 0). This shift between the H_2 molar flow peak and the anodic current peak might be a consequence of the different nature of these processes, i.e., transfer of K^+ ions (fast electrochemical process) and H_2 release (desorption process), and by certain delays in the detection caused by the pipe tubes between the reactor and the gas chromatograph.

Different experiments varying the applied negative current during the H_2 production/storage step under reaction conditions were performed with catalysts Ni_0 and Ni_{80}. During the negative polarization step a higher catalytic activity and a more pronounced deactivation were observed for the catalyst Ni_{80} in comparison to the same experiments performed on Ni_0 (cf. Figure S3 in the Supporting Information), probably due to the higher porosity and gas-exposed surface of the former. These results prove the importance of the porous microstructure of catalyst Ni_{80} in defining the overall electrocatalytic response of the system. Figure 5 shows, for the two Ni catalyst films, the influence of the magnitude of the negative polarization applied during the H_2 production/storage step on both the H_2 release and the positive current density subsequently obtained during the last step of the experiments (i.e., during the linear sweep voltammetry under an Ar atmosphere). The larger amount of released H_2 (6.99×10^{-5} mol of H_2 from sample Ni_{80} vs 5.3×10^{-6} mol of H_2 from

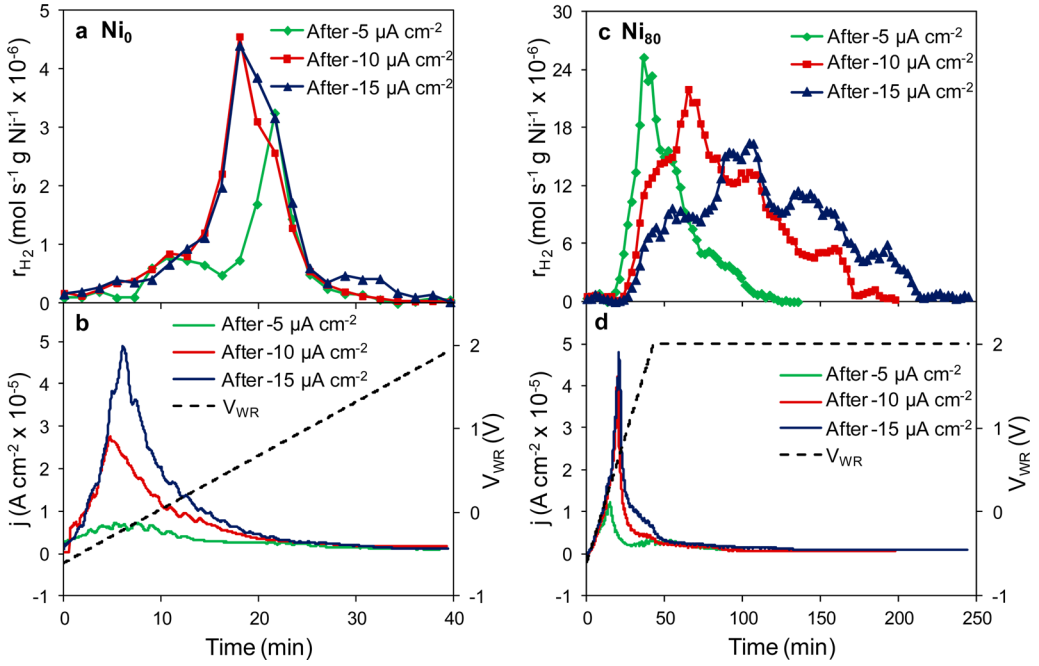

Figure 5. Variation of H_2 molar flow rate and current density (j) with catalyst films (a, b) Ni_0 and (c, d) Ni_{80} at 1 atm and 280 °C during the H_2 release step (100% Ar, LSV from −0.6 V to +2 V, 1 mV s^{-1}) performed after the imposition of different negative currents for 45 min during the H_2 production/storage step (CH_3OH/H_2O = 4.4%/5.2%).

DOI: 10.1021/acscatal.5b02844
ACS Catal. 2016, 6, 1942−1951

sample Ni_0 after applying −15 μA cm^{-2} for 45 min) and the longer duration of the process on sample Ni_{80} further sustain the importance of its peculiar nanostructure in controlling the reactivity of the system. It must be stressed that the amount of transferred K^+ ions transferred to/from the nickel electrode was in all cases much lower than the amount of released H_2, while the amounts of CO and CO_2 released were almost negligible. In terms of amount of hydrogen released per nominal amount of metal, catalysts Ni_{80} and Ni_0 stored up to 19.6 and 0.5 g of H_2 (100 g of Ni)$^{-1}$, respectively: i.e., a H to Ni ratio amounting to 11 for sample Ni_{80}. A first assessment of these figures markedly suggests that not only surface nickel atoms but also other species at the electrode surface participate in the H_2 storage mechanism. Additional experiments carried out subsequently (see Figure S4 in the Supporting Information) strongly supported the carbonaceous nature of these species: (i) methanol feed during the first step of the process was always necessary to achieve a high H_2 storage capacity, (ii) water addition did not produce any significant increase of storage capacity, and (iii) an almost negligible amount of hydrogen was released when the initial negative polarization step was performed under H_2 in an Ar stream. These results also denote that the transferred K^+ ions are not directly bonded to hydrogen, although they affect the H_2 storage/release mechanism, as observed in Figure 5.

A quantitative summary of the main magnitudes entailing these experiments is reported in Table 1, from which is seen the

Table 1. Comparison of Electrochemical Catalyst Performance

	Ni_0 catalyst			Ni_{80} catalyst		
current density during H_2 storage step (μA cm^{-2})	5	10	15	5	10	15
H_2 storage capacity (g of H_2 (100 g of Ni)$^{-1}$)[a]	0.27	0.43	0.49	10.13	19.05	19.59
electric energy consumption (kWh (kg of H_2)$^{-1}$)[b]	0.92	1.28	1.79	0.13	0.15	0.27

[a]These values were obtained from the anodic LSV step. [b]These values include both cathodic and anodic polarization.

remarkably high efficiency of this kind of electrocatalytic system, only requiring a minute electric energy consumption for its operation (ranging from 0.1 to 1.8 kWh (kg of H_2)$^{-1}$). All of the experiments were repeated, and consistent and reproducible results were obtained. For instance, Figure S5 in the Supporting Information confirms the reproducibility of the results obtained in repeated experiments, in terms of overall amounts of released H_2 and transferred K^+. Hence, under such conditions, it is likely that the steady-state conditions have already been reached either in the accumulation degree of graphene oxide or, at least, in its influence on the H_2 storage capacity.

3.3. Surface Chemistry and Role of Potassium Promotion. Scanning electron microscopy was used to examine the surface state of the electrode Ni_{80} before and after its exposure to methanol steam re-forming conditions (Figures 3b,c, respectively). For the fresh catalyst (i.e., before operation), Figure 3b shows the formation of different agglomerates of Ni nanocolumns that leave a considerable free space between them (note that this does not preclude the presence of a thin nickel layer serving as an electrical connection between agglomerates and providing the required electrical conductivity to the ensemble). Interestingly, after the re-forming reaction (CH_3OH/H_2O = 4.4%/5.2%) and an applied potential of V_{WR} = −1 V for 1 h, Figure 3c clearly shows that the space between agglomerates appears fully covered by black regions of pillared fragments of carbonaceous deposits (as determined by EDX) that exhibit a wrinkled and overlapped structure characteristic of graphene oxide (GO).[30,31] This tentative attribution was confirmed by a series of other characterization results as reported next.

XPS spectra (Figure 6a) were recorded for the used catalyst Ni_{80} after positive and negative polarization. In no case it was possible to observe any significant contribution of the alumina substrate, thus confirming that, even in this porous sample, interconnected nickel deposits spread over the entire surface of the ion-conductive pellet. The C 1s spectrum is composed of two well-defined components, one at a binding energy (BE) of 289.4 eV attributed to carbonate/carboxyl-like or similar oxygenated species[32] and another at 284.6 eV usually attributed to C−C bonds that, in their majority, we tentatively recognize as due to the backbone structure of GO. It is remarkable that the K 2p spectrum also reported in this figure (at 292.4 eV for the K $2p_{3/2}$ peak) undergoes a significant decrease in intensity for the sample taken after positive polarization, a feature confirming the electrochemical removal of potassium ions from the catalyst surface back to the solid electrolyte. The Ni 2p peak was also measured after exposure to the atmosphere (Figure S6 in the Supporting Information). In the case of the as-deposited sample, the spectral contribution of the metallic peak at 853 eV is apparent, combined with another component at 855 eV of similar intensity that must be attributed to NiO and/or $Ni(OH)_2$.[33] In the case of the postreaction samples, both of them are very similar, indicating that, after reaction and exposure to the air atmosphere, the nickel surface is at least partially oxidized. However, it should be noted that this technique is only sensitive to a surface thickness of a few nanometers and, thus, no clear conclusions can be drawn from these results in relation to the oxidation state in the bulk of the nanocolumnar Ni catalyst film.

The Raman (Figure 6b) and IR (Figures 6c,d) spectra can be used to identify the carbonaceous species formed on the surface of this catalyst and to follow their evolution upon changing the electrode polarization (i.e., when removing the K^+ ions from the surface). The normalized Raman spectra in Figure 6b are characterized by a series of peaks and bands at 1343, 1597, 2583, and 2895 cm^{-1} which, according to the literature, can be assigned to different vibrational modes of GO. The bands at 1343 and 1597 cm^{-1}, attributed to strong disordered (D) and graphitic (G) vibrational modes and having a intentisty ratio (i.e., I_D/I_G ratio) slightly lower than unity, are generally taken as a fingerprint of GO.[34−36] The less intense bands at 2500−3000 cm^{-1} are also characteristic of graphene oxide.[11,31,34] The high intensity of these Raman peaks, practically the unique clear features observable in the spectra, confirm the assumption that the majority of carbonaceous species formed during the re-forming reaction corresponds to oxidized graphene (cf. Figure 3c). A first noticeable difference between the two Raman spectra, before and after positive polarization (i.e., potassium removal), refers to an increase in the intensity of bands at 2583 (2D) and 2895 (D + G) cm^{-1}, a feature that, according to the literature,[11] must be linked with an increase in the order of the

DOI: 10.1021/acscatal.5b02844
ACS Catal. 2016, 6, 1942−1951

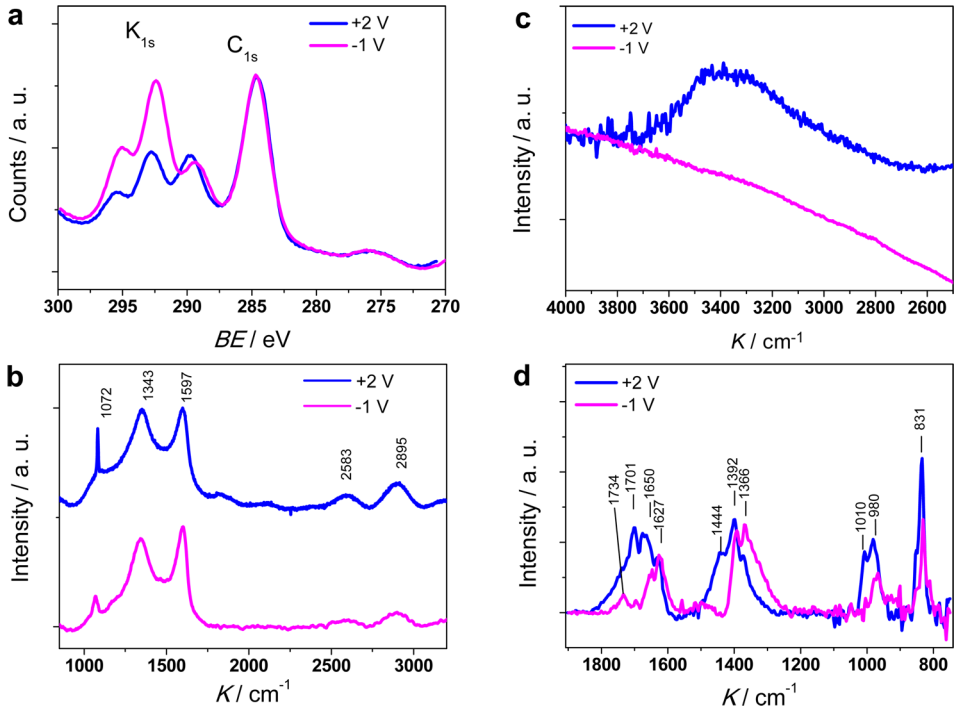

Figure 6. XPS, Raman, and FTIR spectroscopy analysis of catalyst film Ni_{80}: (a) C 1s and K 2p XPS spectra, (b) Raman spectra normalized at the peak 1597 cm^{-1} in the region 3200−2700 cm^{-1}, and (c, d) FTIR spectra in the regions 1900−750 and 4000−2500 cm^{-1}, after application of the Kramer−Kronig correction. Samples were examined after the H_2 production/storage experiments (280 °C, CH_3OH/H_2O = 4.4%/5.2%) and the final application of V_{WR} = −1 V for 1 h (pink lines) and V_{WR} = +2 V for 1 h (blue lines).

graphene structure. Simultaneously, the height increase (the area remaining practically invariable) and sharpening, upon K^+ removal, of the narrow peak at 1072 cm^{-1}, which is the sole band not ascribed to GO but is attributed to the $\nu(CO_3^{2-})$ symmetric stretch of carbonate species,[37] points to a similar increase of the structural order of these adsorbed species.

The FT-IR spectra reported in Figures 6c,d provide additional insights into the evolution of carbonaceous species after positive and negative polarizations. These spectra show a series of bands that, according to the existing literature on graphene oxide and adsorbed carbonate species, can be grouped into five types of functional groups:[31,35,38−40]

(a) broad band around 3400 cm^{-1}: O−H groups
(b) groups of bands around 1700 cm^{-1}: $-COO^-$ antisymmetric stretching, −COOH antisymmetric stretching, −C═O stretching, C═C stretching, adsorbed carbonate species, H_2O
(c) groups of bands around 1390 cm^{-1}: $-COO^-$ symmetric stretching, −OH bending, $-C-O^-$, C−O−C
(d) groups of bands around 1000 cm^{-1}: C−O and C−OH stretching
(e) groups of bands around 830 cm^{-1}: −C-H stretching

The most striking feature when the spectra of the two samples are compared is the appearance of new bands within each group after positive polarization and the clear development of a broad band at around 3400 cm^{-1} due to the stretching of O−H groups. In agreement with the referenced FT-IR studies in the literature on GO, we attribute these changes to the protonation of $C(O)_n$ (n = 1, 2) groups present on the graphene oxide surface after removal of potassium. A reasonable hypothesis agreeing with these changes in the FT-IR spectra and the evolution observed in the Raman spectra is that potassium ions located at the surface of the negatively polarized catalyst contribute to stabilizing both the negatively charged carboxyl and epoxy groups grafted onto the GO and the carbonate groups deposited/adsorbed on the electrode surface. Then, during the removal of potassium from the positively polarized electrode, stabilization of these groups would occur with protons produced in parallel to the observed release of gaseous H_2.

It should also be noted that there are several studies in the literature on the formation of graphitic carbon and graphene sheets from the catalytic decomposition of methane and other hydrocarbons and oxygenated compounds on Ni-based catalysts.[41,42] However, to the best of our knowledge, this is the first time that graphene oxide has been systematically obtained from methanol decomposition in an electrocatalytic system.

4. DISCUSSION

4.1. H_2 Storage and Release Mechanisms. The catalytic performance and the H_2 storage and release results reported in the previous section might involve different chemisorption mechanisms. For example, as supported by XPS and Raman spectra, potassium carbonates or bicarbonates are likely to form under methanol steam re-forming conditions and negative polarization due to the interaction between the K^+ ions and the gaseous molecules present in the reaction mixture (H_2O, H_2, CO_2, and CO).[43,44] Thus, the partial decomposition of adsorbed carbonates during the positive polarization step (see Figure 4a and Figure S3a in the Supporting Information) would probably produce the release of CO and CO_2 and, in the case of bicarbonate species or other methanol steam re-forming intermediates (e.g., methoxy species), also some H_2. However, this mechanism would justify neither the high amount of released hydrogen nor the excess of H_2 with respect to the

DOI: 10.1021/acscatal.5b02844
ACS Catal. 2016, 6, 1942−1951

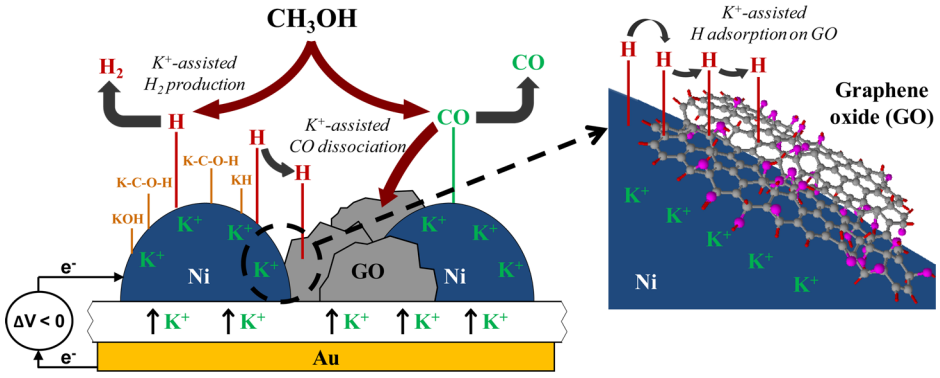

Figure 7. Proposed mechanism for electrochemically assisted H_2 production and storage. Under negative polarization, K^+ ions electrochemically transferred to the nickel catalyst would promote the production of H_2 from methanol and CO dissociation. In addition to the formation of some K^+-derived surface compounds, H_2 would be mainly stored by the K^+-assisted spillover of H atoms on the graphene oxide.

released CO/CO_2. Formation of potassium hydride or hydroxide during the reaction step, another possible way of storing hydrogen,[45] must be also ruled out as the main H_2 storage route, because the amount of transferred K^+ ions transferred to/from the solid electrolyte was in all cases much lower than that of released H_2. Therefore, after discarding these possibilities, we propose here that H_2 storage in this system mainly involves the chemisorption of H atoms on Ni active sites and their spillover onto other surface compounds,[8,9] likely carbonaceous deposits, formed under reaction conditions. Hydrogen spillover is a recursively studied phenomenon in supported catalysts that implies the formation of H atoms by H_2 dissociation[10,11] or H^+ reduction[12,46] on an active catalytic phase and their diffusion to adjacent surface sites over the catalyst support acting as receptor material. The mechanism proposed here to account for H_2 production and storage assumes the occurrence of such a spillover effect on the Ni catalyst film, as schematically illustrated in Figure 7.

Under negative polarization conditions, the incorporation of electropositive alkali ions would modify the electronic state (e.g., work function) of the metal catalyst, leading to significant changes in its chemisorption properties. Specifically, under methanol steam re-forming conditions, the presence of potassium on the catalyst surface likely causes the strengthening of the Ni−C bond and the weakening of the O−H bonds in methanol molecules, thus facilitating the CH_3OH adsorption and posterior dehydrogenation toward H_2 and CO (eqs 3−8).[20,47,48]

$$CH_3OH \rightarrow CH_3OH_{(a)} \quad (3)$$

$$CH_3OH_{(a)} \rightarrow CH_3O_{(a)} + H_{(a)} \quad (4)$$

$$CH_3O_{(a)} \rightarrow H_2CO_{(a)} + H_{(a)} \quad (5)$$

$$H_2CO_{(a)} \rightarrow CO_{(a)} + 2H_{(a)} \quad (6)$$

$$2H_{(a)} \rightarrow H_2 \quad (7)$$

$$CO_{(a)} \rightarrow CO \quad (8)$$

Similarly, as reported in other electrochemical promotion[44] and classical alkali promotion[49] studies, potassium ions would also favor the dissociation of CO molecules and therefore the carbon formation (eq 9).

$$CO_{(a)} \rightarrow C_{(a)} + O_{(a)} \quad (9)$$

The spillover of chemisorbed H atoms would take place from the Ni active sites onto these carbonaceous compounds, where the presence of K^+ ions could stabilize the hydrogen adsorption, as observed elsewhere when alkali ions were intercalated into graphitic layers.[50,51] In these studies, Li- or K-based dopants, among others, acted as electronic promoters to attract hydrogen molecules. A similar K-dependent stabilization would explain in our case that H_2 release only occurred after removal of the K^+ ions from the catalyst film to the solid electrolyte. In agreement with the outlined hypothesis, SEM (Figure 3c), Raman (Figure 6b), and infrared (Figure 6c,d) spectroscopy has demonstrated the formation of graphene oxide (GO) as the main form of carbon species generated from eq 9. The grafting of oxygen-containing groups on the GO is believed to favor the spillover of H atoms[9,52] and its chemisorption in the vicinity of these functional groups or other surface irregularities.[9,53] In this way, this oxidized graphene, decorated with K^+ ions and presenting a rich variety of oxygenated functional groups, would straightforwardly chemisorb hydrogen and would constitute, together with Ni, the main storage recipient of hydrogen in the system. This storage mechanism would also explain the slower H_2 release rate observed for catalyst Ni_{80} in Figure 5c (vs catalyst Ni_0, in Figure 5a), where the reverse spillover of the H adatoms toward the Ni active sites would involve a slower diffusion process of these atoms from rather inaccessible GO sites.

4.2. Assessment of Storage Capacity and Performance of the Electrocatalytic Device. Although there have been several studies on hydrogen production form alcohols by using Ni-based catalysts,[54,55] this is the first time that H_2 has been simultaneously produced and stored by feeding a humidified methanol stream, with the assistance of electrochemistry. Several important particularities and advantages of the proposed electrocatalytic system are listed below. Unlike previous studies where NO_x[56,57] or CO_2[43] were captured by using K^+-conductor solid electrolytes through the formation of, respectively, potassium nitrates and carbonate compounds, K^+ ions in our system would barely be directly bonded to hydrogen, although they would be involved in both the formation of an adsorbent carbonaceous material and the subsequent hydrogen adsorption. Remarkably, the electric energy consumed during the hydrogen storage/release steps was negligible (see Table 1), even if the electrocatalytic system based on Ni_{80} presents H_2 storage capacities as high as 19 wt % with respect to Ni. These values are very encouraging if they are compared, for example, to those obtained with Mg_2NiH_4 (3.6

DOI: 10.1021/acscatal.5b02844
ACS Catal. 2016, 6, 1942−1951

wt %), other hydrides of Ni-containing alloys working at lower operation temperatures, such as $CoNi_5H_4$ and $LaNi_5H_6$ (less than 2 wt %), and even the best-performing hydrides, i.e., the borohydrides (around 18 wt %), which typically require decomposition temperatures as high as 600 °C for hydrogen release.[4−6]

The use of oblique angle physical vapor deposited films for H_2 storage in the form of MgH_2 was reported for V-decorated and V-doped Mg nanostructures.[21,58] In these studies, H_2 adsorption and desorption temperatures generally decreased upon increasing the zenithal deposition angle,[21] and the theoretical hydrogen storage capacity for MgH_2 (7.6 wt %) was reached at around 280 °C.[58] However, in those and most studies in the literature on the storage of hydrogen, this gas is fed in molecular form, thus requiring the previous implementation of ex situ hydrogen production processes. Moreover, in the commonly employed storage systems based on either H_2 physisorption or formation of metal hydrides, pressure and/or temperature have to be modified during adsorption/desorption steps to enable the uptake/release of the gas. It is remarkable that the Ni/K-βAl_2O_3/Au electrochemical catalysts developed here enable the direct (in situ) H_2 production and storage under fixed, mild operation conditions (280 °C and atmospheric pressure), with the electrical polarization as the unique control parameter. Hence, in this system, hydrogen is supplied neither from a gaseous stream nor from an aqueous solution but as the product of an internal methanol re-forming reaction simultaneously carried out on the porous Ni catalyst film. We believe that the developed electrocatalytic system shows potential applications for the in situ controlled storage and release of hydrogen under fixed, mild reaction conditions from fuels such as methanol. In view of the obtained results, one could even consider the possibility of implementing this process by using similar electrocatalytic systems composed of nickel catalyst films deposited on both sides of the alkali-conductor material, in such a way that both the production/storage and the release of H_2 could be continually (cyclically) carried out by only switching the electric polarization.

5. CONCLUSIONS

The present work faces two important challenges in the current development of hydrogen technology: H_2 production from sustainable sources and its efficient storage. An advanced electrocatalytic system has been developed, on the basis of porous nickel catalyst films with tunable microstructure which were prepared by the oblique angle physical vapor deposition technique on a K^+-conductor material acting as catalyst support. The electrochemical catalysts were tested under methanol steam re-forming conditions for the simultaneous K^+-assisted H_2 production and storage.

The key roles of both the catalyst porosity and K^+ ion transfer in H_2 storage (and release) were proved. The deposition of graphene oxide on the catalyst surface under the reaction conditions also seemed to be of paramount importance in enhancing the H_2 storage capacity of the system. On the basis of the experimental results and several characterization techniques, a H_2 storage mechanism has been proposed mainly on the basis of hydrogen chemisorption on nickel active sites and its spillover onto the graphene oxide aggregates under the promotional effect of K^+ ions.

With respect to most of the common H_2 storage systems based on either physisorption or chemisorption processes, three major advantages of this electrocatalytic system must be highlighted:

(1) An unparalleled hydrogen storage capacity per amount of metal is obtained (up to 19 g of H_2 (100 g of Ni)$^{-1}$) under relatively mild conditions (280 °C, 1 atm) and with negligible electric energy consumption (less than 2 kWh kg H_2^{-1}).
(2) Hydrogen is not fed in its molecular form or by electrochemical means. H_2 is simultaneously obtained and stored by feeding a humidified methanol stream as raw material.
(3) No change in temperature or pressure is required in the whole process. Hydrogen production, storage, and release are carried out under fixed operation conditions, by only varying the applied current or potential.

■ ASSOCIATED CONTENT

Supporting Information

The Supporting Information is available free of charge on the ACS Publications website at DOI: 10.1021/acscatal.5b02844.

Additional SEM images and XPS spectra, further experiments of hydrogen storage/release performed with catalyst Ni_0 for comparison with catalyst Ni_{80} (cf. Figure 4), and results obtained with catalyst Ni_{80} under different reaction atmospheres and in consecutive sets of experiments (reproducibility test) (PDF)

■ AUTHOR INFORMATION

Corresponding Author

*A.d.L.-C.: tel, +34-926295300; fax, +34-926295437; e-mail, Antonio.lconsuegra@uclm.es.

Present Address

§(J.G.-C.) Institute of Chemical Research of Catalonia, Ave. Paisos Catalans 16, 43007 Tarragona, Spain. E-mail address: jcobos@iciq.es.

Notes

The authors declare no competing financial interest.

■ ACKNOWLEDGMENTS

The authors gratefully acknowledge the Spanish Ministry of Economy and Competiveness (projects MAT2013-40852-R, MAT2013-42900-P, and CTQ2013-45030-R) for the financial support of this work.

■ REFERENCES

(1) Holladay, J. D.; Hu, J.; King, D. L.; Wang, Y. *Catal. Today* **2009**, *139*, 244−260.
(2) Palo, D. R.; Dagle, R. A.; Holladay, J. D. *Chem. Rev.* **2007**, *107*, 3992−4021.
(3) Zanchet, D.; Santos, J. B. O.; Damyanova, S.; Gallo, J. M. R.; Bueno, J. M. C. *ACS Catal.* **2015**, *5*, 3841−3863.
(4) Dalebrook, A. F.; Gan, W.; Grasemann, M.; Moret, S.; Laurenczy, G. *Chem. Commun.* **2013**, *49*, 8735−8751.
(5) Van Den Berg, A. W. C.; Areán, C. O. *Chem. Commun.* **2008**, *6*, 668−681.
(6) Schlapbach, L.; Züttel, A. *Nature* **2001**, *414*, 353−358.
(7) Chen, H. Y. T.; Tosoni, S.; Pacchioni, G. *ACS Catal.* **2015**, *5*, 5486−5495.
(8) Prins, R. *Chem. Rev.* **2012**, *112*, 2714−2738.
(9) Psofogiannakis, G. M.; Froudakis, G. E. *Chem. Commun.* **2011**, *47*, 7933−7943.
(10) Wang, L.; Yang, F. H.; Yang, R. T.; Miller, M. A. *Ind. Eng. Chem. Res.* **2009**, *48*, 2920−2926.

DOI: 10.1021/acscatal.5b02844
ACS Catal. 2016, 6, 1942−1951

(11) Pham, V. H.; Dang, T. T.; Singh, K.; Hur, S. H.; Shin, E. W.; Kim, J. S.; Lee, M. A.; Baeck, S. H.; Chung, J. S. *J. Mater. Chem. A* **2013**, *1*, 1070−1077.
(12) Krishna, R.; Titus, E.; Costa, L. C.; Menezes, J. C. J. M. D. S.; Correia, M. R. P.; Pinto, S.; Ventura, J.; Araújo, J. P.; Cavaleiro, J. A. S.; Gracio, J. J. A. *J. Mater. Chem.* **2012**, *22*, 10457−10459.
(13) Toda, K.; Furue, R.; Hayami, S. *Anal. Chim. Acta* **2015**, *878*, 43−53.
(14) Hegab, H. M.; Zou, L. *J. Membr. Sci.* **2015**, *484*, 95−106.
(15) Meng, F.; Cushing, S. K.; Li, J.; Hao, S.; Wu, N. *ACS Catal.* **2015**, *5*, 1949−1955.
(16) Byun, J. *J. Microbiol. Biotechnol.* **2015**, *25*, 145−151.
(17) Matthew, M.; Hawkeye, M. T.; Taschuk, M. J. B. *Glancing Angle Deposition of Thin Films: Engineering the Nanoscale*; Wiley: Chichester, U.K., 2014; pp 1−80.
(18) Barranco, A.; Borrás, A.; González-Elipe, A. R.; Palmero, A. *Prog. Mater. Sci.* **2016**, *76*, 59−153.
(19) Kariuki, N. N.; Khudhayer, W. J.; Karabacak, T.; Myers, D. J. *ACS Catal.* **2013**, *3*, 3123−3132.
(20) González-Cobos, J.; Rico, V. J.; González-Elipe, A. R.; Valverde, J. L.; de Lucas-Consuegra, A. *Catal. Sci. Technol.* **2015**, *5*, 2203−2214.
(21) He, Y.; Fan, J.; Zhao, Y. *Int. J. Hydrogen Energy* **2010**, *35*, 4162−4170.
(22) González-García, L.; Parra-Barranco, J.; Sánchez-Valencia, J. R.; Barranco, A.; Borrás, A.; González-Elipe, A. R.; García-Gutiérrez, M. C.; Hernández, J. J.; Rueda, D. R.; Ezquerra, T. A. *Nanotechnology* **2012**, *23*, 205701−205710.
(23) Rico, V.; Romero, P.; Hueso, J. L.; Espinós, J. P.; González-Elipe, A. R. *Catal. Today* **2009**, *143*, 347−354.
(24) Rico, V.; Borrás, A.; Yubero, F.; Espinós, J. P.; Frutos, F.; González-Elipe, A. R. *J. Phys. Chem. C* **2009**, *113*, 3775−3784.
(25) Vayenas, C. G.; Bebelis, S.; Pliangos, C.; Brosda, S.; Tsiplakides, D. *Electrochemical Activation of Catalysis: Promotion, Electrochemical Promotion and Metal-Support Interactions*; Kluwer Academic Publishers/Plenum Press: New York, 2001; pp 1−10.
(26) Vernoux, P.; Lizarraga, L.; Tsampas, M. N.; Sapountzi, F. M.; De Lucas-Consuegra, A.; Valverde, J. L.; Souentie, S.; Vayenas, C. G.; Tsiplakides, D.; Balomenou, S.; Baranova, E. A. *Chem. Rev.* **2013**, *113*, 8192−8260.
(27) Whitacre, J. F.; Rek, Z. U.; Bilello, J. C.; Yalisove, S. M. *J. Appl. Phys.* **1998**, *84*, 1346−1353.
(28) Bayca, S. U.; Cansizoglu, M. F.; Biris, A. S.; Watanabe, F.; Karabacak, T. *Int. J. Hydrogen Energy* **2011**, *36*, 5998−6004.
(29) Iwasa, N.; Yoshikawa, M.; Nomura, W.; Arai, M. *Appl. Catal., A* **2005**, *292*, 215−222.
(30) Sobon, G.; Sotor, J.; Jagiello, J.; Kozinski, R.; Zdrojek, M.; Holdynski, M.; Paletko, P.; Boguslawski, J.; Lipinska, L.; Abramski, K. M. *Opt. Express* **2012**, *20*, 19463−19473.
(31) Ho, C. Y.; Liang, C. C.; Wang, H. W. *Colloids Surf., A* **2015**, *481*, 222−228.
(32) Hueso, J. L.; Espinós, J. P.; Caballero, A.; Cotrino, J.; González-Elipe, A. R. *Carbon* **2007**, *45*, 89−96.
(33) Grosvenor, A. P.; Biesinger, M. C.; Smart, R.St.C.; McIntyre, N. S. *Surf. Sci.* **2006**, *600*, 1771−1779.
(34) Kim, H. J.; Lee, S. M.; Oh, Y. S.; Yang, Y. H.; Lim, Y. S.; Yoon, D. H.; Lee, C.; Kim, J. Y.; Ruoff, R. S. *Sci. Rep.* **2014**, *4*, 5176−5185.
(35) Perera, S. D.; Mariano, R. G.; Vu, K.; Nour, N.; Seitz, O.; Chabal, Y.; Balkus, K. J. *ACS Catal.* **2012**, *2*, 949−956.
(36) Serrano-Lotina, A.; Daza, L. *Appl. Catal., A* **2014**, *474*, 107−113.
(37) Xu, C.; Reed, R.; Gorski, J. P.; Wang, Y.; Walker, M. P. *J. Mater. Sci.* **2012**, *47*, 8035−8043.
(38) Hou, H.; Hu, X.; Liu, X.; Hu, W.; Meng, R.; Li, L. *Ionics* **2015**, *21*, 1919−1923.
(39) Acik, M.; Lee, G.; Mattevi, C.; Chhowalla, M.; Cho, K.; Chabal, Y. J. *Nat. Mater.* **2010**, *9*, 840−845.
(40) Galande, C.; Mohite, A. D.; Naumov, A. V.; Gao, W.; Ci, L.; Ajayan, A.; Gao, H.; Srivastava, A.; Bruce Weisman, R.; Ajayan, P. M. *Sci. Rep.* **2011**, *1*, 85−89.
(41) Lavin-Lopez, M. P.; Valverde, J. L.; Ruiz-Enrique, M. I.; Sanchez-Silva, L.; Romero, A. *New J. Chem.* **2015**, *39*, 4414−4423.
(42) Abbas, H. F.; Wan Daud, W. M. A. *Int. J. Hydrogen Energy* **2010**, *35*, 1160−1190.
(43) Ruiz, E.; Cillero, D.; Morales, Á.; Vicente, G. S.; De Diego, G.; Martínez, P. J.; Sánchez, J. M. *Electrochim. Acta* **2013**, *112*, 967−975.
(44) Urquhart, A. J.; Keel, J. M.; Williams, F. J.; Lambert, R. M. *J. Phys. Chem. B* **2003**, *107*, 10591−10597.
(45) Simonyan, V. V.; Johnson, J. K. *J. Alloys Compd.* **2002**, *330*−*332*, 659−665.
(46) Mukherjee, S.; Ramalingam, B.; Gangopadhyay, S. *J. Mater. Chem. A* **2014**, *2*, 3954−3960.
(47) Neophytides, S.; Vayenas, C. G. *J. Catal.* **1989**, *118*, 147−163.
(48) Kusche, M.; Enzenberger, F.; Bajus, S.; Niedermeyer, H.; Bösmann, A.; Kaftan, A.; Laurin, M.; Libuda, J.; Wasserscheid, P. *Angew. Chem., Int. Ed.* **2013**, *52*, 5028−5032.
(49) Joyner, R. W.; van Santen, R. A. *Elementary Reaction Steps in Heterogeneous Catalysis*; Springer: Dordrecht, The Netherlands, 2012; pp 324−325.
(50) Zabel, H.; Solin, S. A. *Graphite Intercalation Compounds II: Transport and Electronic Properties*; Springer-Verlag: Berlin, Heidelberg, 2013; pp 128−135.
(51) Deng, W. Q.; Xu, X.; Goddard, W. A. *Phys. Rev. Lett.* **2004**, *92*, 166103.
(52) Li, Q.; Lueking, A. D. *J. Phys. Chem. C* **2011**, *115*, 4273−4282.
(53) Kayanuma, M.; Nagashima, U.; Nishihara, H.; Kyotani, T.; Ogawa, H. *Chem. Phys. Lett.* **2010**, *495*, 251−255.
(54) Fatsikostas, A. N.; Verykos, X. E. *J. Catal.* **2004**, *225*, 439−452.
(55) Mei, D.; Dagle, V. L.; Rong, X.; Albrecht, K.; Dagle, R. A. *ACS Catal.* **2016**, *6*, 315−325.
(56) de Lucas-Consuegra, A.; Caravaca, Á.; Sánchez, P.; Dorado, F.; Valverde, J. L. *J. Catal.* **2008**, *259*, 54−65.
(57) de Lucas-Consuegra, A.; Caravaca, A.; Martín de Vidales, M. J.; Dorado, F.; Balomenou, S.; Tsiplakides, D.; Vernoux, P.; Valverde, J. L. *Catal. Commun.* **2009**, *11*, 247−251.
(58) He, Y.; Zhao, Y. *Nanotechnology* **2009**, *20*, 204008−204018.

DOI: 10.1021/acscatal.5b02844
ACS Catal. 2016, 6, 1942−1951